Applied Catalysis B: Environmental 304 (2022) 120987

Contents lists available at ScienceDirect

Applied Catalysis B: Environmental

journal homepage: www.elsevier.com/locate/apcatb

Iron-cation-coordinated cobalt-bridged-selenides nanorods for highly efficient photo/electrochemical water splitting

Shumaila Ibraheem [a,b], Ghulam Yasin [a,b,*], Anuj Kumar [c], Muhammad Asim Mushtaq [a], Sehrish Ibrahim [d], Rashid Iqbal [a,b], Mohammad Tabish [e], Sajjad Ali [f], Ali Saad [a,b]

[a] Institute for Advanced Study, Shenzhen University, Shenzhen 518060, Guangdong, China
[b] Institute of Microscale Optoelectronics, Shenzhen University, Shenzhen 518060, Guangdong, China
[c] Nano-Technology Research Laboratory, Department of Chemistry, GLA University, Mathura, Uttar Pradesh 281406, India
[d] College of Life Science and Technology, Beijing University of Chemical Technology, Beijing 100029, China
[e] State Key Laboratory of Chemical Resource Engineering, Beijing University of Chemical Technology, Beijing 100029, China
[f] Department of Physics, Southern University of Science and Technology, Shenzhen 518055, China

ARTICLE INFO

Keywords:
Photo/electrochemical water splitting
Synergistic electrocatalysis
Oxygen evolution reaction
Hydrogen evolution reaction
Fe-coordinated Co-Se-bridging-bond

ABSTRACT

Water-electrolysis intends a favorable green technology to hold the worldwide energy and ecological disaster, but its efficacy is significantly restricted by the slow reaction kinetics of both the anodic oxygen evolution reaction (OER) and cathodic hydrogen evolution reaction (HER). Herein, the fabrication of multi-cation incorporated $Fe^{2+/3+}/Co^{2+}$ species into selenides nanorods (Fe@Co/Se_2-NRs) and corresponding analysis of their catalytic activity for electrochemical (EC) and solar-driven water splitting as a purpose of the composition are reported. This efficient approach can fabulously endow electronic structure modulation and the direct evidence of electron-transfer-route between transition-metals and selenides, which are vital to improving the electrocatalytic activity, has never been confirmed before. For the first time, we explored the electron-transfer route of intensely-coupled Fe@Co/Se_2-NRs catalyst, in which the $Fe^{2+/3+}/Co^{2+}$ species strongly-coupled to selenide through the Fe-coordinated Co-bridged-bond. Finally, density functional theory calculations disclose that the multi-cation doping effects into selenides are vital for enhanced electrocatalytic performance.

1. Introduction

Electrochemical (EC) and photo-electrochemical (PEC) water splitting comprise of oxygen evolution reaction (OER) [1–4] and hydrogen evolution reaction (HER) [5,6] signifies the most favorable ways for the renewable energy conversion and storage technologies [7–15]. However, the sluggish kinetics of both the cathodic (HER) and anodic (OER) reactions cause vast energy penalties, which significantly obstruct the commercial application of this water-electrolysis green technology [16–21]. The recent research pays efforts on exploring the efficient bifunctional electrocatalysts that can overwhelm the slow kinetics as well as hasten the evolution rates of O_2 and H_2 at low overpotentials [22–24]. So far, sufficient types of water-splitting electrocatalysts covering noble metals such as Ir/Ru-based (OER active) [25], Pt-based (HER active) [26] materials and transition metal-based catalysts [27] have been developed. Nonetheless, as OER and HER are diverse in reaction mechanisms [28], yields and optimal operating conditions, the inconsistency of two different electrodes in a single water electrolysis device might result in lower the efficiency of the catalyst, and typically a catalyst good for OER does not achieve well in HER, and vice versa [29]. Regarding this, it is still challenging to develop the bifunctional catalysts which are active for both OER and HER simultaneously for overall water splitting. The efficiently prepared bifunctional catalyst will critically simplify the device fabrication process and lower the capital cost.

Over the past years, countless struggles have been waged to develop the transition-metal based bifunctional catalysts including metal oxides [30], metal hydroxides [31], metal nitrides [32], metal phosphides [33], metal sulfides [34], metal selenides [35] and metal chalcogenides [36], etc. However, these bifunctional electrocatalysts are commonly fabricated with robust performance in one reaction whereas improving the catalytic activity in the other reaction [37–39]. Among these non-noble metal-based nanomaterials, metal-selenides (M-Se_x M = Fe, Co, Ni, etc.) are considered as favorable candidates with an appropriate d-electron configuration [40]. For instance, density functional theory (DFT)

* Corresponding author at: Institute for Advanced Study, Shenzhen University, Shenzhen 518060, Guangdong, China.
E-mail address: yasin@mail.buct.edu.cn (G. Yasin).

https://doi.org/10.1016/j.apcatb.2021.120987
Received 16 August 2021; Received in revised form 30 October 2021; Accepted 28 November 2021
Available online 3 December 2021

calculations illustrate that the Se atoms-sites at the edges of M-Se_x are HER active sites [41]. It is broadly accepted that the electrocatalytic activity of selenides can be boosted by doping different metals and generating matrix vacancies to exploit the integer of edge-active centers [42]. Besides, it is revealed that the various metallic cations doping in selenides improve the catalytic activity due to the synergistic contributions from different metal cations [43]. Indeed, incorporating the metal cations into selenides can tempt atomic spins due to strain and increase the exposed active sites [44]. However, other concerns like an agglomeration of nanoparticles due to doping methodologies and blockage of active centers are unavoidable during the catalyst preparation, which pointers the worst ion diffusivity and chemical interaction [22,45]. Likewise, the electronic modulation mechanism during catalyst reaction remains elusive, particularly in heterogeneous-metal doped selenides composite materials, which critically forbids the fabrication and development of highly competent and robust bifunctional electrocatalysts for overall water splitting to yield molecular hydrogen [46]. In this situation, it is anticipated that the incorporation of foreign cations into selenides could be highly effective in modifying the electronic interaction and lattice structure and, hence further improving the catalytic activity [47]. Up to now, there have been rare reports on explaining the electronic-modulation mechanism during the reaction for overall water splitting process.

In this motivation, we reported a novel class of organized synthesis of dual-metal-cations coordinated selenides (M_x-Se_x, M = Fe and Co) via in situ hydrothermal coordinative self-templated strategy using metal salts as cation source. This strongly-coupled iron-cation-coordinated and cobalt-bridged Fe@Co/Se_2 nanorods (NR) catalyst avoids the agglomeration of nanorods and can trigger competent overall water splitting owing to the resilient electronic interfacial relation among the metal atoms and selenides. The X-ray photoelectron spectroscopy (XPS), extended X-ray absorption fine structure spectroscopy (EXAFS) and DFT simulations investigation specifies the stouter electronic modulation and bridging among the cations and selenides, which is favorable to enhancing the adsorption energy of reaction intermediates. Consequently, this novel Fe-coordinated Co-bridged selenide nanorods catalyst (Fe@Co/Se_2-NRs) shows outstanding catalytic performance for both HER (78 mV at 10 mA cm^{-2}) and OER (overpotential of 200 mV at 10 mA cm^{-2}). When this Fe@Co/Se_2-NRs catalyst is engaged as both the cathode/anode reactions for overall EC-water-splitting, only 1.51 V cell voltage is vital to reach @10 mA cm^{-2} current density. While coupled with a silicon-photovoltaic-cell for PEC-water-splitting, this Fe@Co/Se_2-NRs catalyst facilitates independent continuous operation for ~3 days with a solar-to-hydrogen conversion efficacy of ~ 7.0%. We assume that such a metal-cation doping approach can also be applied to other chalcogenide composites in order to prevent agglomeration and induce significant electronic modulations to replace commercial Pt/C&IrO_2 for various energy technologies.

2. Experimental

2.1. Fabrication of Fe-Se_2

Typically, solution A was prepared by dissolving iron (II) chloride tetrahydrate (0.1655 g) in 0.5 M EDTA (10 mL) and sonicates it for about 20 min. Solutions B was prepared by dispersing Se metal powder (0.32 g) in 3.3 M sodium hydroxide solution (30 mL) and sonicate it for about 20 min. After then solution B was added to solution A under strong magnetic stirring. After dynamic stirring for 5–10 min, the mixed solution was further transferred into Teflon and the mixed solution is hydrothermally treated at 180 °C for about 26 h. The precipitates were collected by centrifugation and followed by subsequent ethanol washing and drying at 75 °C overnight. The product was collected as Fe-Se_2 and saved for further use and characterization.

2.2. Fabrication of Co-Se_2

Typically, solution A was prepared by dissolving cobalt (II) Chloride hexahydrate (0.3956 g) in 0.5 M EDTA (10 mL) and sonicates it for about 20 min. Solution B was prepared by dispersing Se metal powder (0.32 g) in 3.3 M sodium hydroxide solution (30 mL) and sonicate it for about 20 min. After then solution B was added to solution A under strong magnetic stirring. After dynamic stirring for 5–10 min, the mixed solution was further transferred into Teflon and the mixed solution is hydrothermally treated at 180 °C for about 26 h. The precipitates were collected by centrifugation and followed by subsequent ethanol washing and drying at 75 °C overnight. The product was collected as Co-Se_2 and saved for further use and characterization.

2.3. Fabrication of Fe@Co/Se_2-nanorods

Typically, solution A was prepared by dissolving iron (II) chloride tetrahydrate (0.1655 g) and cobalt (II) chloride hexahydrate (0.3956 g) and in 0.5 M EDTA (20 mL) (Fe/Co molar ratio was adjusted as 1:2) and sonicate it for about 30 min. Solution B was prepared by dispersing Se metal powder (0.32 g) in 3.3 M sodium hydroxide solution (30 mL) and sonicate it for about 20 min. After then solution B was added to solution A under strong magnetic stirring. After dynamic stirring for 5–10 min, the mixed solution was further transferred into Teflon and the mixed solution is hydrothermally treated at 180 °C for about 26 h. The precipitates were collected by centrifugation and followed by subsequent ethanol washing and drying at 75 °C overnight. The product was collected as Fe@Co/Se_2-nanorods and saved for further use and characterization.

3. Results and discussion

3.1. Physicochemical characterization

The novel Fe, Co dual-cation doped selenide Fe@Co/Se_2-nanorods (NRs) were synthesized by controlled one-step hydrothermal treatment using the in-situ coordinative-self-templated strategy as shown in Fig. 1a, and the details of the synthetic procedure are given in the supplementary information. Specifically, the feed content of metal salts of $FeCl_2{\cdot}4H_2O$ and $CoCl_2{\cdot}6H_2O$ (molar ratio of 1:2) were used as dual-cation Fe^{2+}/Co^{2+} source in Se metal powder solution, which directs to the formation of the Fe@Co/Se_2-nanorods catalyst. Thanks to the virtuous affinity between selenide and $Fe^{2+/3+}/Co^{2+}$ ions, which leads to the formation of uniform interconnected nanorods symmetry, which is favorable to a radical improvement in catalytic activity via electronic modulation [48]. The distinctive nanorods shape for the Fe@Co/-Se_2-NRs catalyst can clearly be observed from scanning electron microscopy (SEM) images (Fig. 1b_1-b_2). This uniform nanorodic shape formation is due to adjusting the Fe^{2+}/Co^{2+} ratio via an in-situ coordinated self-template approach which is beneficial to expose more edge/surface active sites and prevent agglomeration of nanoparticles faced in usual synthesis methodologies of transition metal nanoparticles. This unique nanorodic morphology of Fe@Co/Se_2-NRs catalyst is also confirmed by the transmission electron microscopy (TEM) image shown in Fig. 1c. It is consistent with the SEM annotations that the Fe, Co dual-cation doped selenides are the nanorods structure with smooth edges and surfaces. The correlating high-resolution TEM (HRTEM) image displays well-determined lattice-fringes with inter-planar distances of 2.6 Å consistent to the (1 1 1) planes of Co-Se_2 and Fe-Se_2 (Fig. 1d and S13). To reveal the crystalline phase of the as-obtained Fe@Co/Se_2-NRs catalyst, the X-ray diffraction (XRD) analysis was carried out (Fig. 1f). And the XRD data of Fe@Co/Se_2-NRs catalyst exposes the specific peaks at 23.0°, 30.8°, 34.6°, 36.0°, 47.8°, 50.4°, 53.5° and 63.3° are assigned to the (1 1 0), (1 0 1), (1 1 1), (1 2 0), (2 2 0), (0 0 2), (0 3 1) and (3 1 1) lattice planes agreed well with the standard $CoSe_2$ (JCPDS: 00-053-0449). Considering the analogous pattern of $FeSe_2$

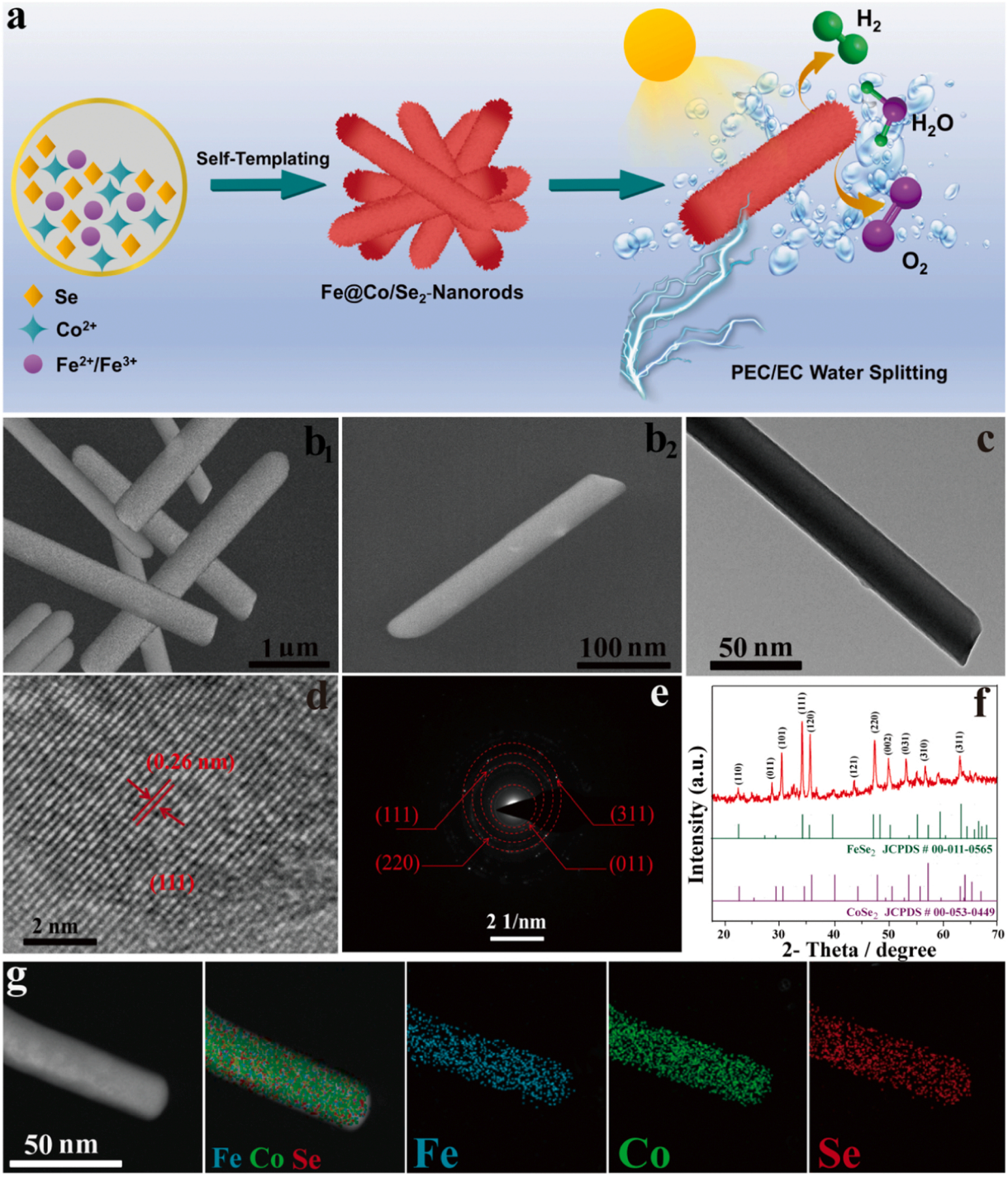

Fig. 1. (a) Graphic illustration for the synthetic route of Fe@Co/Se_2-NRs catalyst. (b_1-b_2) FESEM images of the Fe@Co/Se_2-NRs catalyst. (c) TEM image of the Fe@Co/Se_2-NRs catalyst. The HRTEM image (d) and the resultant SAED pattern (e) of the Fe@Co/Se_2-NRs catalyst. (f) XRD pattern of Fe@Co/Se_2-NRs catalyst. (g) HAADF-STEM image of the Fe@Co/Se_2-NRs sample and the resultant elemental mapping images of Fe, Co and Se elements.

(JCPDS: 00-011-0565) to $CoSe_2$ and the consistent composition dispersal in the Fe@Co/Se_2-NRs nanostructures. The Fe-coordinated Co-Se_2 nanorods formation was also confirmed by HRTEM and resultant selected area electron diffraction (SAED) analysis (Fig. 1e). The inter-planar distance of the attained sample was about 2.6 Å, 1.40 Å, 1.86 Å, and 3.07 Å representing the (1 1 1), (3 1 1), (2 2 0) and (0 1 1) lattice-planes of Fe@Co/Se_2-NRs catalyst, respectively, which are very well consistent with the crystal structure facts obtained from the XRD data of the Fe@Co/Se_2-NRs catalyst.

The scanning TEM (STEM) and the resulting energy dispersive X-ray (EDX) mapping of the Fe@Co/Se_2-NRs electrocatalyst confirm the occurrence of Fe, Co and Se elements in the Fe@Co/Se_2-NRs catalyst (Fig. 1g). It is obviously witnessed that all the constituents (i.e., Fe, Co, and Se) display homogenous distribution across the nanorods, validating that the Fe^{2+}/Co^{2+} dual-cation are successfully doped simultaneously in selenide and well enriched with the surface active sites and make porous Fe@Co/Se_2-NRs without crystal-structure collapse throughout the in-situ hydrothermal process. Moreover, the porosity of the as-obtained catalysts was analyzed by N_2 adsorption-desorption isotherms (Fig. S1a), from which the Brunauer-Emmertt-Teller (BET) specific

surface area and pore-volume of Fe-Se_2, Co-Se_2, and Fe@Co/Se_2-NRs were resolute to be 73.23 m^2 g^{-1} and 0.14 cm^3g^{-1}, 81.40 m^2 g^{-1} and 0.15 cm^3 g^{-1} and 104.56 m^2 g^{-1} and 0.21 cm^3 g^{-1}, respectively (Table S3). On the equivalent size-distribution curves, the discrete maxima focused at about 3.28, 4.67, and 5.65 nm can be detected for Fe-Se_2, Co-Se_2, and Fe@Co/Se_2-NRs, respectively (Fig. S1b). The porous structure not only proposes a higher BET specific surface area and more active centers, but also accelerates the transmission of the electrolyte and the expulsion of gas-bubbles which is an important factor to higher the catalytic performance [49].

The XPS measurements were conceded to examine the chemical status, elemental compositions and valence state information of as-obtained Fe-Se_2, Co-Se_2, and Fe@Co/Se_2-NRs catalysts. The XPS survey-spectrum further validated the existence of Fe, Co and Se elements in Fe@Co/Se_2-NRs catalyst (Fig. S2) and the atomic surface-contents are layouts in Table S1. The inductively-coupled-plasma mass-spectrometry (ICP-MS) examination showed the weight-constituents of Fe, Co and Se for Fe@Co/Se_2-NRs catalyst were determined to be 11.84 wt%, 25.98 wt% and 13.02 wt%, respectively (Table S2), which is agreed well with the XPS analysis results. The imperative fact we would like to acquire from XPS analysis is the unique electronic structure modulation after co-doping of selenide. Considerably, the synergistic effects, robust coupling interaction and electron transference route can be evidently seen from the high-resolution core-spectrum of Fe $2p_{3/2}$, Co $2p_{3/2}$ and Se 3d. The mono-cation-doped selenides i.e., Fe-Se_2 and Co-Se_2 display a negligible XPS peak shift equated with that of dual-cation-doped selenides (Fig. 2). Generally, the XPS peak modification of the dual-cation-doped catalyst redirects electronic configuration modulation and potential electron transfer among cations, representing the occurrence of the strong electronic interface between each component after metallic atom doping.

Furthermore, we found that the resultant binding energy (B.E) of Fe $2p_{3/2}$ at 707.97 eV in Fe@Co/Se_2-NRs catalyst superbly shifted to higher B.E 709.76 eV as compared with the Fe $2p_{3/2}$ in Fe-Se_2 (Fig. 2c), and the subsequent B.E of Co $2p_{3/2}$ at 778.05 eV in Fe@Co/Se_2-NRs catalyst finely shifted to lower B.E 777.19 eV as compared with the Co $2p_{3/2}$ in Co-Se_2 (Fig. 2d). This positive and negative shift in B.Es of Fe $2p_{3/2}$ and Co $2p_{3/2}$, respectively, showed the resilient electron transfer among cations, which means iron gives electrons to cobalt element in this catalyst, which is consistent to the order of the electronegativity of Fe and Co is: Fe < Co. Metal-element with superior electronegativity has the stout capacity to fascinate electrons; this is reliable with the statistic that the Co XPS-peak moves to lower B.Es in Fe@Co/Se_2-NRs. The peak position and peak area of Fe 2p and Co 2p change significantly after double doping (Table S8-S9), which further verified the robust electron transfer process among catalysts. However, we also found that the corresponding B.Es of Se $3d_{3/2}$ and Se $3d_{5/2}$ at 55.82 eV and 54.81 eV in Fe@Co/Se_2-NRs catalyst shifted to lower B.Es at 54.86 eV and 53.87 eV in comparison to Fe-Se_2 (Fig. 2e). Interestingly, we can observe that only Fe-cation doping into selenides has almost negligible electronic interaction, whereas the Fe^{2+}/Co^{2+} doping has great electronic interaction on Se XPS peaks, demonstrating the bridging-effect of Cobalt in Fe@Co/Se_2-NRs catalyst. This strong Fe-coordinated Co-bridged selenide creates higher cationic vacancies usually revealing favorable catalytic performance triggering functionalities [50].

The valence-state and coordination-atmosphere of the Fe/Co element in Fe@Co/Se_2-NRs catalyst were further analyzed by the X-ray absorption near-edge spectroscopy (XANES) and EXAFS. The XANES spectral examination showed that the Fe K-edge (Fig. 2a) and Co K-edge (Fig. S3a) own the threshold absorption position starting at 7109 eV and

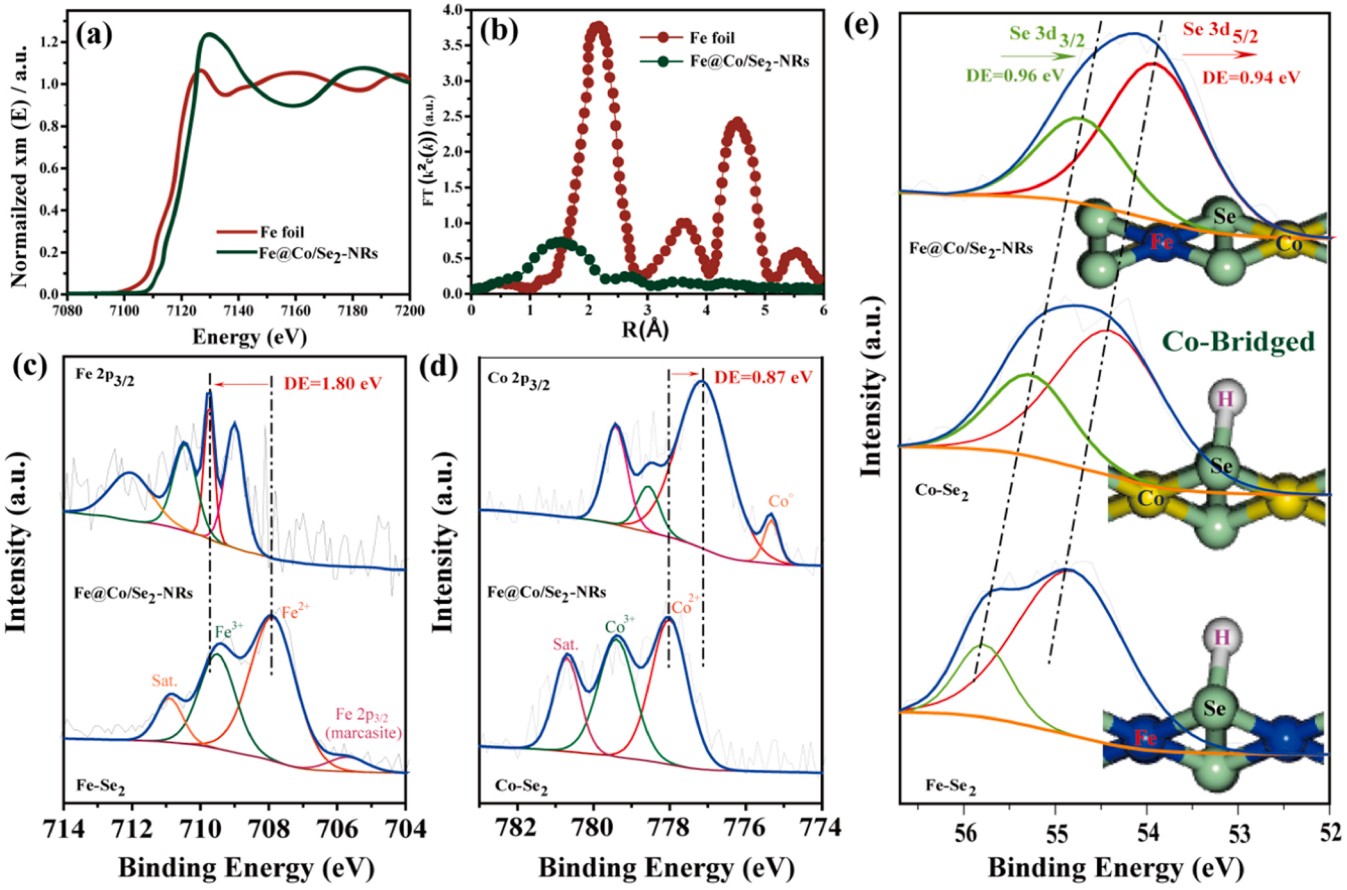

Fig. 2. XANES Fe K-edge spectra (a) and Fe K-edge Fourier transforms (FTs) EXAFS spectra (of the k^2-weighted (k) functions) (b) of the Fe@Co/Se_2-NRs and Fe foil. High resolution XPS spectra of Fe $2p_{3/2}$ (c), Co $2p_{3/2}$ (d) and Se 3d (e).

7705 eV, respectively and also calibrated with pure Fe-foil and Co-foil signifying the +2/+3 valance-state of Fe-species and +2 valance-state of Co-species in the Fe@Co/Se_2-NRs catalyst. The Fourier transforms EXAFS (FT-EXAFS) spectral analysis of Fe (Fig. 2b) and Co (Fig. S3b) exposed that the Fe@Co/Se_2-NRs possess Fe-Co and Co-Se coordination with sharp peaks. It is also worth noting that there is no corresponding peak of Fe-Fe and Co-Co in Fe and Co foil, respectively in Fe@Co/Se_2-NRs catalyst. This result clearly confirmed that the prevailing-mode of Fe@Co/Se_2-NRs is Fe-coordinated and Co-Se-bridged bond rather than the Se-Fe/Se-Se/Fe-Fe/Co-Co coordination relations.

3.2. Electrocatalytic performance towards OER/HER

Considering the highly desired features, a rotating disk electrode (RDE) was used to estimate the electrocatalytic performances by steady-state linear sweep voltammetry (LSV) curves of the as-made catalysts for both the OER/HER in alkaline media. The activity-enhancement of $Fe^{2+/3+}/Co^{2+}$ doped selenides can be clearly seen from the OER electrocatalytic performance of the as-obtained catalysts, which is explored by sweeping the RDE potential ranging from 1.23 to 1.8 V in 1.0 M KOH, and the subsequent LSV-curves are shown in Fig. 3a. The Fe@Co/Se_2-NRs electrocatalyst delivers the lowermost overpotential (200 mV) at the current density of 10 mA cm^{-2}, which is even much inferior to its counter-samples Fe-Se_2 (360 mV), Co-Se_2 (250 mV) and IrO_2 (320 mV) (Fig. 3i and S4a). Meanwhile, the basic kinematic factor is the Tafel slope to explore the rate-determining footstep of an electrochemical procedure. Commonly, the OER mechanism in alkaline media comprises of four-electron transferal route. The Fe@Co/Se_2-NRs catalyst exposed an inferior Tafel slope (35 mV/dec) than its counterparts Fe-Se_2 (105 mV/dec), Co-Se_2 (65 mV/dec) and IrO_2 (95 mV/dec) (Fig. 3b), signifying the outstanding electronic-transferal rate of OER and increased active centers for OH^- adsorption on this distinctive Fe@Co/Se_2-NRs catalyst [51]. The turnover frequency (TOF) is also an imperative factor to analyze the intrinsic features of electrocatalytical performance [52]. Herein, it is devised that all the metal-sites are electrochemically active in Fe@Co/Se_2-NRs throughout the

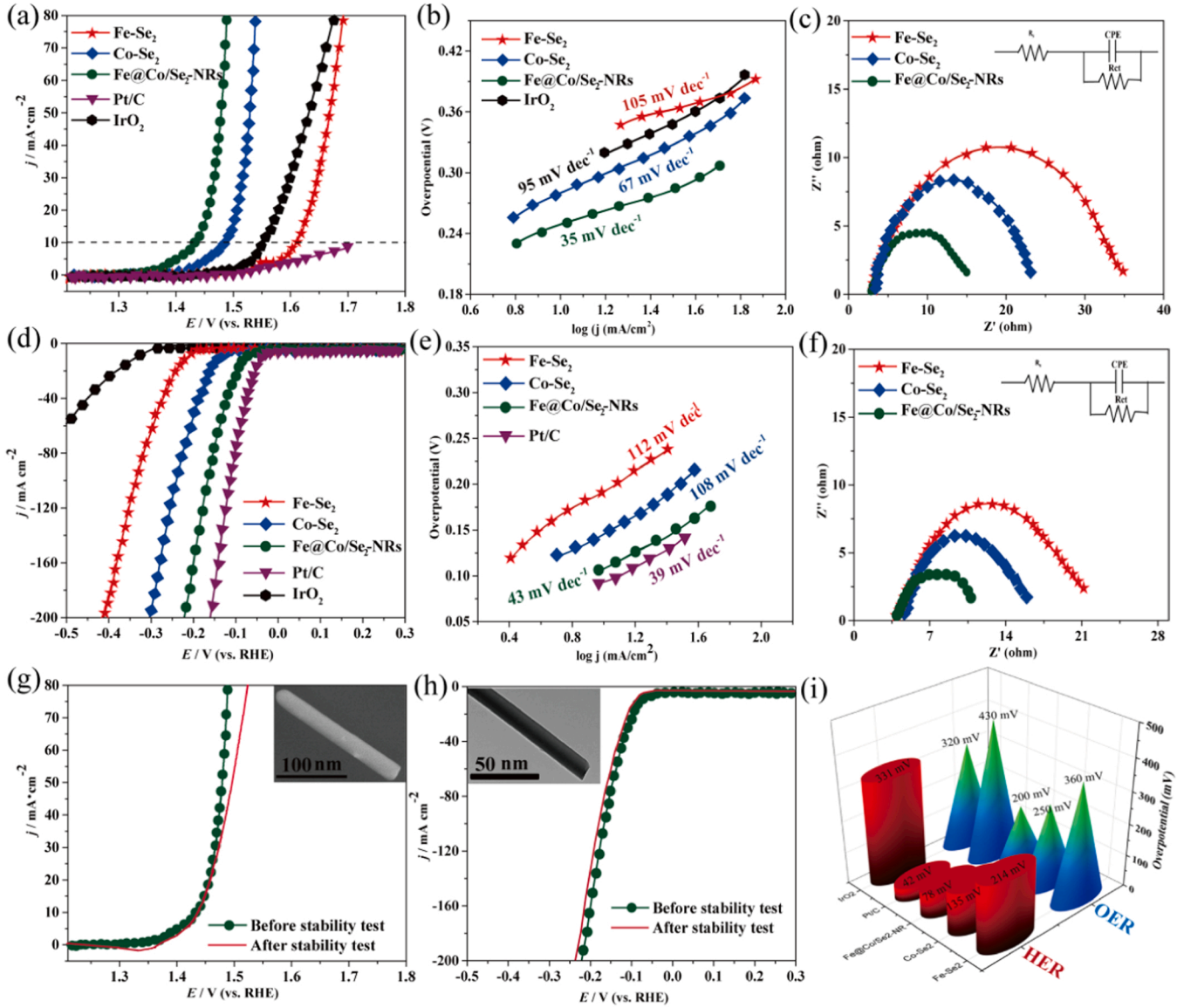

Fig. 3. 95% iR optimized OER LSV curves (a) and the corresponding Tafel slope (b) of Fe-Se_2, Co-Se_2, Fe@Co/Se_2-NRs, Pt/C and IrO_2 catalysts noted in 1.0 M KOH solution at 10 mVs^{-1}. HER polarization curves (d) and corresponding Tafel slope (e) of Fe-Se_2, Co-Se_2, Fe@Co/Se_2-NRs, Pt/C and IrO_2 catalysts noted in 1.0 M KOH solution at 10 mVs^{-1}. Nyquist plots for the OER (c) and HER (f) of Fe-Se_2, Co-Se_2, Fe@Co/Se_2-NRs catalysts. OER (g) and HER LSV curves (h) of Fe@Co/Se_2-NRs before and after 2000 cycles. (i) Overpotentials for both OER/HER calculated from corresponding polarization curves at 10 mA cm^{-2} of Fe-Se_2, Co-Se_2, Fe@Co/Se_2-NRs, Pt/C and IrO_2 catalysts.

water-splitting process. The Fe@Co/Se_2-NRs catalyst has 0.611 s^{-1} TOF per site at 250 mV overpotential, which is higher than Co-Se_2 (0.534 s^{-1}) and Fe-Se_2 (0.242 s^{-1}). This higher TOF value of Fe@Co/-Se_2-NRs further verified its outstanding activity towards OER. Additionally, electrochemical impedance spectroscopy (EIS) analysis was accompanied to better understand the electrode-kinetics throughout the OER mechanism. It can be notice from Nyquist plots (Fig. 3c), the Fe@Co/Se_2-NRs catalyst shows a smaller charge-transfer resistance (Rct) than those of Fe-Se_2 and Co-Se_2, further signifying the fast kinetic route as directed by the smallest Tafel slope.

To characterize the bi-functionality of the Fe@Co/Se_2-NRs electrocatalyst and other counterparts, the HER catalytic performance was also evaluated in 1.0 M KOH. As exposed in Fig. 3d, the steady-state LSV curve of Fe@Co/Se_2-NRs clearly demonstrates that at the current density of 10 mA cm^{-2}, the Fe@Co/Se_2-NRs catalyst has an overpotential of 78 mV much lesser than the Co-Se_2 (135 mV), Fe-Se_2 (214 mV) and little higher to commercial Pt/C (42 mV) (Fig. 3i and S4b), indicating the robust HER performance for the Fe@Co/Se_2-NRs electrode. Moreover, the corresponding Tafel plot is fit to be 43 mV dec^{-1} for the Fe@Co/Se_2-NRs electrode, which is the lowest equated to other counterparts (Fig. 3e). Smaller Tafel plot standards are promising for commercial applications due to it relates to high gas-evolution rates at certain overpotentials. Yet again, analogous to the OER mechanism, the EIS data exposed that the Fe@Co/Se_2-NRs electrode has the lowermost impedance for Rct (Fig. 3f and Table S4), which is in agreement with the chief kinetics triggered by the $Fe^{2+/3+}$, Co^{2+} multi-doping of selenides. We also compare the catalytic activities of Fe@Co/Se_2-NRs towards both OER/HER, while using the graphite electrode and Pt as the counter electrode, and we found that all the corresponding activities are comparable (Fig. S5a-b).

Besides, good catalytic-activity, the durability of the catalysts towards both OER/HER is important for commercializing it into various energy conversion and storage technologies. The robustness of Fe@Co/Se_2-NRs electrode for both OER/HER was evaluated by 2000 cyclic-voltammetry (CV) cycles. The corresponding polarization-curve for both HER (Fig. 3h) and OER (Fig. 3g) revealed negligible difference compared to the primary ones with only 0.5% loss in the current-density. However, the long-term stability of the Fe@Co/Se_2-NRs catalyst towards both the OER/HER was also tested by chronopotentiometry (CP) measurements. The Fe@Co/Se_2-NRs catalyst could retains its constant overpotential for 20 h at a set current density of 10 mA cm^{-2} for OER (Fig. S6a) and only 0.3% loss of overpotential for HER after 20 h (Fig. S6b) at 10 mA cm^{-2} current density. These results confirmed that the Fe@Co/Se_2-NRs have good OER/HER performance and durability in basic media. Moreover, to evaluate the robustness of morphology, crystalline structure, and elemental composition of Fe@Co/Se_2-NRs catalyst, the SEM, HRTRM, EDS mapping, XRD and XPS measurements were carried out after the stability test. From the SEM and HRTEM images, it can be endorsed that the physical structure after the stability test remains unchanged (Fig. S7a-b). The SEM and corresponding EDS mapping images (Fig. S7c), and XPS investigation (Fig. S8) convey the conclusive proof that the Fe@Co/Se_2-NRs catalyst is chemically stable and presents all the elements after the stability test. And the XRD data (Fig. S9) after the stability test validates the crystalline-phase constancy of this Fe@Co/Se_2-NRs catalyst.

Based on the above outcomes, the outstanding bifunctional OER/HER electrocatalytic performance can be attributed to our $Fe^{2+/3+}$/Co^{2+} co-doped selenides nanorods-based electrode to the subsequent reasons. First, the unique interconnected porous conductive nanorods morphology affords high active surface area, while the $Fe^{2+/3+}$/Co^{2+} incorporation has increased surface-active centers due to the increased degree of covalency in lattice [53]. Second, the resilient electronic-interaction due to Fe-coordination and Co-bridged selenides related with a prime adsorption energy of reaction-intermediates boosts the catalytic performance. Third, the interconnected nanorodic-array assembly not only accelerates the electron transference processes and diffusion of electrolyte, but also quickens the discharge of evolved gas-effervesce, which pointers to prompt kinetics. It is designated that the Fe@Co/Se_2-NRs-based electrode has outstanding OER/HER activity and stability than the commercial Pt/C&IrO_2-based electrodes and other reported catalysts (Table S4-S6).

3.3. Photo/electrochemical water splitting of Fe@Co/Se_2-NRs

Motivated by the robust OER/HER catalytic performance of our Fe@Co/Se_2-NRs electrode, we then made a full water electrolyzer using Fe@Co/Se_2-NRs as both the anode/cathode in 1.0 M KOH (Fig. 4e). There is only 1.51 V cell voltage is required to reach at 10 mA cm^{-2} current density and this condition could maintain to 2500 cycles with negligible degradation (Fig. 4a). The galvanostatic-testing process was also used to evaluate the stability for overall water splitting. The water electrolysis at three current densities (10, 20 and 50 mA cm^{-2}) was accompanied successively for about 30 h (Fig. 4b), and the stable resultant voltage at each current-density was found. The Faradic-efficacy for both the OER/HER mechanism was measured by equating the theoretical volume of evolved-gas with the experimental-value as counted by the water-drainage mode. The anode/cathode illustrates constant oxygen/hydrogen evolution-rates that agreed well with theoretical standards, entail an approximately 100% Faradic efficiency of the Fe@Co/Se_2-NRs-based water electrolyzer shown in the inset of Fig. 4a. So, our rationally fabricated electro-catalyst can trigger good efficacy and durability towards electrical water splitting (Table S7).

Finally, the electrocatalytic activity of this bifunctional Fe@Co/Se_2-NRs catalyst in PEC-water-splitting is exhibited. A commercial Si-solar cell was used as to transform the solar irradiation (AM 1.5 G virtual sunlight) into electrical energy. The PEC-performance of Fe@Co/Se_2-NRs catalyst is first assessed by polarization curves under virtual solar light (Fig. S10). The obtained photo-current density of Fe@Co/Se_2-NRs in a light-off environment is insignificant but upon illumination, the PEC performance of Fe@Co/Se_2-NRs shows a substantial shift and reaches an onset-potential of 0.18 V and a noticeable increase in the photocurrent density as well. To evaluate the independent PEC overall water-splitting, the solar-cell was electrically coupled to the Fe@Co/Se_2-NRs electrodes shown in Fig. 4e. A current density of 5.40 mA cm^{-2} was noted down from this PEC-water-splitting device, which was durable with the repeated light OFF-ON cycles of virtual AM 1.5 G sunlight brightness (Fig. 4c), indorsing that Fe@Co/Se_2-NRs efficiently lifts the PEC performance of Si solar-cell. Negligible deprivation in the current density was detected after 72 h of continuous operation; the oxygen and hydrogen bubbles were progressively formed and released from the Fe@Co/Se_2-NRs electrode surface throughout the process (Fig. 4d). The incident photon-to-current efficiency (IPCE) was measured under photo illumination (Oriel Cornerstone 130 monochromator used as a monochromatic light source) at 1.23 V vs RHE, and power output was determined via a photodiode detector. The Fe@Co/Se_2-NRs proved to be an effective photoelectrocatalyst for water splitting theoretically and experimentally. The photocurrent density of Fe@Co/Se_2-NRs (5.40 mA cm^{-2} at 1.23 V) showed remarkable increment as compared to the pristine Co-Se_2 (3.21 mA cm^{-2} at 1.23 V) and Fe-Se_2 (2.83 mA cm^{-2} at 1.23 V), signifying the electronic structure alternation and improved light-harvesting capability of photoanode by Fe-doping (Fig. S14a). The photocurrent density of Fe@Co/Se_2-NRs is twice higher than the pristine Co-Se_2 and Fe-Se_2 close to the obtained current density of Co-catalyzed $BiVO_4$ photoanodes [54]. Significantly, the Fe@Co/Se_2-NRs demonstrated superior IPCE values over Co-Se_2 and Fe-Se_2 from the UV to visible light region (up to 540 nm). The IPCE of the Fe@Co/Se_2-NRs is 49.5% at 380 nm, which is significantly greater than Co-Se_2 (29.3%) and Fe-Se_2 (24.7%). The increase in IPCE is associated with the enhanced light absorption of Fe@Co/Se_2-NRs (Fig. S14b).

UV–visible spectroscopy was employed to study the photocatalytic response of Fe-Se_2, Co-Se_2 and strongly-coupled Fe@Co/Se_2-NRs. The Fe-Se_2 and Co-Se_2 demonstrated the light absorption in the near cyan

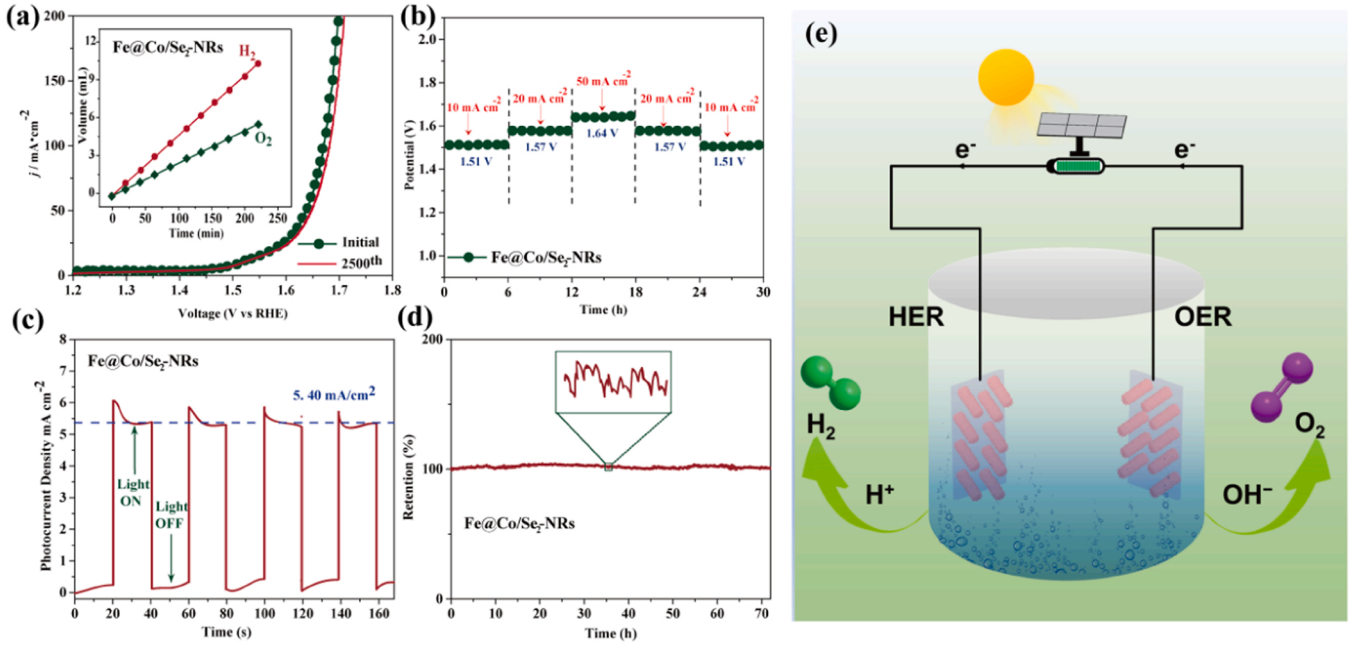

Fig. 4. (a) Polarization curve of Fe@Co/Se_2-NRs catalyst for overall water splitting before and after 2500 CV cycles at 5 mVs^{-1} in 1.0 M KOH (inset illustrates the produced (symbols) and calculated (lines) capacities of H_2/O_2 as a function of time). (b) Multi-current track carried out at different current densities for long-term stability of Fe@Co/Se_2-NRs catalyst. (c) Chrono-amperometric *i-t* measurement of the Fe@Co/Se_2-NRs catalyst (solar water splitting cell) under chopped simulated illumination (AM 1.5 G). (d) Photocurrent density retention of water splitting cell under constant sunlight illumination for ~ 3 days. (e) Graphical presentation of photo/electro-chemical overall water splitting cell with as-obtained Fe@Co/Se_2-NRs catalyst.

region whereas the absorption edge of Fe@Co/Se_2-NRs showed an obvious red shift of visible light spectrum, representing the boost in light absorption capability of the $Fe^{2+/3+}/Co^{2+}$ species containing strongly-coupled Fe@Co/Se_2-NRs (Fig. S15a). In addition, the optical bandgap energy of Fe-Se_2 (2.83 eV), Co-Se_2 (2.78 eV) and Fe@Co/Se_2-NRs (2.66 eV) was determined using UV–vis absorption spectra of the catalytic materials (Fig. S15b). The red-shift in the absorption edge of Fe@Co/Se_2-NRs indicates the significant narrowing of bandgap, owing to the excessive generation and reduced recombination rate of photo-generated charge carriers, the higher light-harvesting capability, and

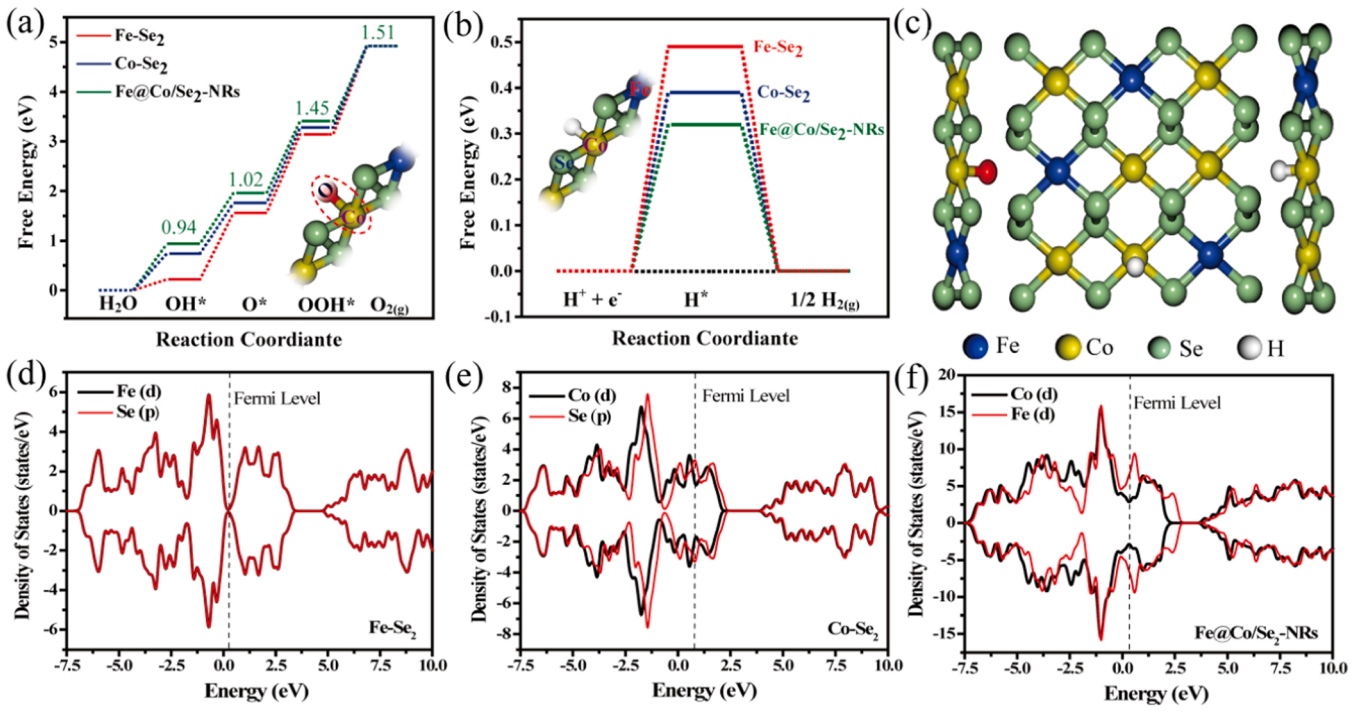

Fig. 5. (a) OER Gibbs free-energy graphs for the four-step reactions on Fe-Se_2, Co-Se_2 and Fe@Co/Se_2-NRs samples (inset shows the molecular structure with O adsorption on Co site of Co-Se_2). (b) HER Gibbs free-energy diagrams of the Fe-Se_2, Co-Se_2 and Fe@Co/Se_2-NRs samples (inset shows the molecular structure with Fe-coordinated Co-Se_2 active sites of Fe@Co/Se_2-NRs). (c) The top and side vision of Fe@Co/Se_2-NRs surface. The projected density of state of pristine Fe-Se_2 (d), Co-Se_2 (e) and Fe@Co/Se_2-NRs (f) catalysts.

thus increasing the photocatalytic activity of Fe-coordinated Co-bridged-selenide nanorods during PEC water splitting [55,56]. A solar light-to-hydrogen (STH) conversion competence of ~ 7.0% was acquired (Fig. S16a-b), which can be additionally improved by using superior solar-cells with optimized operating circumstances. This could be credited to morphological and intrinsic electronic engineering of Fe@Co/Se_2-NRs, which warranties the effective utilization of external light as well. Considering the highly desirable features, it is appreciated to fabricate such noble-metal free alternatives to advance the photo/electro-chemical hydrogen production.

3.4. Mechanistic study on OER/HER of bifunctional Fe@Co/Se_2-NRs

To gain additional comprehensions into the OER/HER catalytic processes of Fe@Co/Se_2-NRs, we executed DFT simulation using first principle calculation techniques to govern the electronic structures and catalytic reaction mechanisms for the $Fe^{2+/3+}$, Co^{2+} co-doped selenides structures (Fig. 5). To evaluate the OER/HER catalytic performance of these materials, all probable forms of doping structure (i.e. Fe-Se_2 and Co-Se_2) were fabricated to further disclose the influence of metal doping sites. A constant large spreading of the density of states (DOS) across the Fermi level of Fe@Co/Se_2-NRs (Fig. 5c and f) was appeared as compared to Fe-Se_2 (Fig. 5d and S11a-c) and Co-Se_2 (Fig. 5e), resulting in the significant enhancement in electrical conductivity of $Fe^{2+/3+}$, Co^{2+} co-doped selenides than other counterparts. Further, to assess HER, three states were demonstrated; (i) H^+ state, (ii) intermediate H* state, and (iii) catalyst-1/2H_2 state. Gibbs free-energy change for intermediate adsorbed hydrogen (ΔG_{H^*}) is an important criterion for HER [57] and the ΔG_{H^*} between both steps (ii) and (iii) as above should be small as close as possible to zero for the ideal catalyst. Therefore, the value of ΔG_{H^*} was calculated for all Fe-Se_2, Co-Se_2 and Fe@Co/Se_2-NRs samples and found to be 0.49 eV, 0.39 eV and 0.32 eV on Fe, Co and Co sites, respectively (Fig. 5b). These outcomes strongly recommended that Co atoms in Fe@Co/Se_2-NRs become more active towards HER after Fe-coordination in Co-Se_2, endowing the dual metal doping interaction towards significant improvement in intrinsic HER activity.

For OER, the DFT calculations indicated that Co-Se_2 and Fe-Se_2 materials have less electrical conductivity with a bandgap value of 0.41 eV and 0.95 eV, respectively, whereas, in the case of Fe@Co/Se_2-NRs sample possess high electrical conductivity of Co-Se_2 reducing the bandgap value from 0.41 to 0.29 eV, verifying the $Fe^{2+/3+}$, Co^{2+} co-doped selenides can facilitate the fast electron transfer process (Fig. 5a). This difference in charge density distribution was supposed to be responsible for fast electron transfer from Co to Se after Fe-introduction in Co-Se_2, further verifying the Fe-coordination cobalt bridged selenides bond in Fe@Co/Se_2-NRs. However, systematic DFT calculations were also accomplished of all samples by optimizing all O-intermediates on every model for the OER investigation. The results suggested that in all cases, the formation of *OOH intermediate from *O state involved high free energy, therefore, this step can be considered as the rate-determining step during OER [58]. However, Fe@Co/Se_2-NRs involved less free energy, i.e., 1.51 eV, as compared to Fe-Se_2 (1.78 eV) and Co-Se_2 (1.64 eV), which strongly indicated the easy detachment of formed O_2 from the active site, endowing enhancement in OER activity of Co-Se_2 after Fe-coordination and reduced the energy barriers for rate-determining step validating the fastening of OER kinetics on Fe@Co/Se_2-NRs. Based on the above analysis of Fe doping effects on the electrocatalytic activity of Fe@Co/Se_2-NRs, considering Co as the active site, we also performed similar calculations on this catalyst by supposing Fe as the active site (Figs. S12a-b). The results indicated that Fe@Co/-Se_2-NRs possessed enhanced HER as well as OER as compared to $FeSe_2$ but less than $CoSe_2$ and Fe@Co/Se_2-NRs catalysts, indicating that Fe@Co/Se_2-NRs is the best performing catalyst having Co as the main active site for the overall water splitting. The enhanced catalytic HER/OER activity of Fe@Co/Se_2-NRs may be attributed to the favorable adsorption-desorption behavior and faster HER/OER kinetics caused by the Fe-doping into $CoSe_2$.

4. Conclusions

In summary, we successfully demonstrated a simple and efficient strategy to synthesize the novel Fe@Co/Se_2-NRs as highly-active and stable electrocatalyst for both OER/HER mechanisms via the controlled one-step in-situ hydrothermal treatment of which the unique morphologies, electronic structures modulations and moderated activities are credited to the incorporated $Fe^{2+/3+}$/Co^{2+} species into selenides. Remarkably, for the first-time we displayed comprehensive evidence of the electron-transference route via Fe-coordinated Co-bridged-bond in selenides. As verified by TEM, XPS and EXAFS capacitive analysis of as-obtained Fe@Co/Se_2-NRs endow distinct porous nature, enhanced exposure of surficial active sites, and interconnected conducting-networks for fast electron transference, feature higher adsorption-facility to the oxygenated intermediates accountable for improving both the OER/HER activities. Epitomized by incorporation of $Fe^{2+/3+}$/Co^{2+} species into selenides has considerably dropped the overpotentials for both OER (200 mV@10 mA cm^{-2}) and HER (78 mV@10 mA cm^{-2}) with high durability of 20 h. A full-cell made from the Fe@Co/Se_2-NRs catalyst as both the anode/cathode for electrical water-splitting only requires a cell-voltage of 1.51 V to reach at 10 mA cm^{-2}. Furthermore, when integrated with Si-solar cells for PEC water-splitting, the Fe@Co/Se_2-NRs can expressively improve the performance of PEC hydrogen-production. The first principle DFT calculations exposed that the multi-cation doping into selenides is vital to engendering bifunctional OER/HER activity. Our work delivers novel insights into modifying the morphology and electronic structure of transition metal-based selenides and offers implications in designing the highly-competent and low-cost bifunctional electrocatalysts for various applications in energy storage/conversion dedications.

CRediT authorship contribution statement

S. Ibraheem: Conducted experiments, Synthesis & characterization, Writing – review & editing. **A. Kumar: DFT calculations, Formal analysis, Writing – review & editing. M.A. Mushtaq:** DFT calculations, Formal analysis, Writing – review & editing. **S. Ibrahim:** Characterization, Formal analysis and writing. **R. Iqbal:** Formal analysis. **M. Tabish:** Formal analysis, Writing – review & editing. **S. Ali:** Discussion, Writing – review & editing. **A. Saad:** Discussion, Writing – review & editing. **G. Yasin:** Project administration, Writing – review & editing.

Declaration of Competing Interest

The authors declare that they have no known competing financial interests or personal relationships that could have appeared to influence the work reported in this paper.

Acknowledgments

We acknowledge the financial support from the China Postdoctoral Science Foundation. We are also thankful for the infrastructural support from the Shenzhen University and Beijing University of Chemical Technology.

Appendix A. Supporting information

Supplementary data associated with this article can be found in the online version at doi:10.1016/j.apcatb.2021.120987.

References

[1] B.-J. Kim, X. Cheng, D.F. Abbott, E. Fabbri, F. Bozza, T. Graule, I.E. Castelli, L. Wiles, N. Danilovic, K.E. Ayers, N. Marzari, T.J. Schmidt, Highly active

nanoperovskite catalysts for oxygen evolution reaction: insights into activity and stability of Ba0.5Sr0.5Co0.8Fe0.2O2+δ and PrBaCo2O5+δ, Adv. Funct. Mater. 28 (2018), 1804355.
[2] L. Yang, Z. Liu, S. Zhu, L. Feng, W. Xing, Ni-based layered double hydroxide catalysts for oxygen evolution reaction, Mater. Today Phys. 16 (2021), 100292.
[3] S. Ibraheem, G. Yasin, R. Iqbal, A. Saleem, T.A. Nguyen, S. Ibrahim, 6 - Silicon-based nanomaterials for energy storage, in: S. Thomas, T.A. Nguyen, M. Ahmadi, G. Yasin, N. Joshi (Eds.), Silicon-Based Hybrid Nanoparticles, Elsevier, 2022, pp. 103–124.
[4] R. Gao, D. Yan, Recent development of Ni/Fe-Based micro/nanostructures toward photo/electrochemical water oxidation, Adv. Energy Mater. 10 (2020), 1900954.
[5] B. Zhu, R. Zou, Q. Xu, Metal–organic framework based catalysts for hydrogen evolution, Adv. Energy Mater. 8 (2018), 1801193.
[6] T. Wu, J. Hong, Z. Lu, H. Wu, C. Wu, Z. Tang, X. Liu, B. Zeng, Y. Xu, G. Chen, C. Yuan, L. Dai, In-situ generation of Ru-catechol coordinative polymer precursor for high-performance hydrogen evolution reaction doped carbon catalyst, Appl. Catal. B: Environ. 285 (2021), 119795.
[7] S. Ibraheem, S. Chen, J. Li, W. Li, X. Gao, Q. Wang, Z. Wei, Three-dimensional Fe, N-decorated carbon-supported NiFeP nanoparticles as an efficient bifunctional catalyst for rechargeable zinc–O2 batteries, ACS Appl. Mater. Interfaces 11 (2019) 699–705.
[8] G. Yasin, S. Ibrahim, S. Ibraheem, S. Ali, R. Iqbal, A. Kumar, M. Tabish, Y. Slimani, T.A. Nguyen, H. Xu, W. Zhao, Defective/graphitic-synergy in heteroatom-interlinked-triggered metal-free electrocatalyst for high-performance rechargeable Zinc-Air, Batter., J. Mater. Chem. A (2021).
[9] Q. Wang, S. Chen, P. Li, S. Ibraheem, J. Li, J. Deng, Z. Wei, Surface Ru enriched structurally ordered intermetallic PtFe@PtRuFe core-shell nanostructure boosts methanol oxidation reaction catalysis, Appl. Catal. B: Environ. 252 (2019) 120–127.
[10] M. Arif, G. Yasin, L. Luo, W. Ye, M.A. Mushtaq, X. Fang, X. Xiang, S. Ji, D. Yan, Hierarchical hollow nanotubes of NiFeV-layered double hydroxides@CoVP heterostructures towards efficient, pH-universal electrocatalytical nitrogen reduction reaction to ammonia, Appl. Catal. B: Environ. 265 (2020), 118559.
[11] R. Gao, H. Zhang, D. Yan, Iron diselenide nanoplatelets: stable and efficient water-electrolysis catalysts, Nano Energy 31 (2017) 90–95.
[12] W. Ye, M. Arif, X. Fang, M.A. Mushtaq, X. Chen, D. Yan, Efficient photoelectrochemical route for the ambient reduction of N2 to NH3 based on nanojunctions assembled from MoS2 nanosheets and TiO2, ACS Appl. Mater. Interfaces 11 (2019) 28809–28817.
[13] G. Yasin, M. Arif, T. Mehtab, X. Lu, D. Yu, N. Muhammad, M.T. Nazir, H. Song, Understanding and suppression strategies toward stable Li metal anode for safe lithium batteries, Energy Storage Mater. 25 (2020) 644–678.
[14] M.A. Mushtaq, M. Arif, X. Fang, G. Yasin, W. Ye, M. Basharat, B. Zhou, S. Yang, S. Ji, D. Yan, Photoelectrochemical reduction of N2 to NH3 under ambient conditions through hierarchical MoSe2@g-C3N4 heterojunctions, J. Mater. Chem. A 9 (2021) 2742–2753.
[15] X. Gao, S. Chen, J. Deng, S. Ibraheem, J. Li, Q. Zhou, H. Lan, X. Zou, Z. Wei, High temperature self-assembly one-step synthesis of a structurally ordered PtFe catalyst for the oxygen reduction reaction, Chem. Commun. 55 (2019) 12028–12031.
[16] M. Nadeem, G. Yasin, M.H. Bhatti, M. Mehmood, M. Arif, L. Dai, Pt-M bimetallic nanoparticles (M = Ni, Cu, Er) supported on metal organic framework-derived N-doped nanostructured carbon for hydrogen evolution and oxygen evolution reaction, J. Power Sources 402 (2018) 34–42.
[17] M. Nadeem, G. Yasin, M. Arif, H. Tabassum, M.H. Bhatti, M. Mehmood, U. Yunus, R. Iqbal, T.A. Nguyen, Y. Slimani, H. Song, W. Zhao, Highly active sites of Pt/Er dispersed N-doped hierarchical porous carbon for trifunctional electrocatalyst, Chem. Eng. J. 409 (2021), 128205.
[18] F. Han, S. Yun, J. Shi, Y. Zhang, Y. Si, C. Wang, N. Zafar, J. Li, X. Qiao, Efficient dual-function catalysts for triiodide reduction reaction and hydrogen evolution reaction using unique 3D network aloe waste-derived carbon-supported molybdenum-based bimetallic oxide nanohybrids, Appl. Catal. B: Environ. 273 (2020), 119004.
[19] A. Kumar, D.K. Das, V.K. Vashistha, S. Ibraheem, G. Yasin, S. Gautam, V. Sharma, A novel CoN4-driven self-assembled molecular engineering for oxygen reduction reaction, Int. J. Hydrogen Energy 46 (2021) 26499–26506.
[20] R. Gao, J. Zhu, D. Yan, Transition metal-based layered double hydroxides for photo (electro)chemical water splitting: a mini review, Nanoscale 13 (2021) 13593–13603.
[21] G. Yasin, M. Arif, T. Mehtab, M. Shakeel, M.A. Mushtaq, A. Kumar, T.A. Nguyen, Y. Slimani, M.T. Nazir, H. Song, A novel strategy for the synthesis of hard carbon spheres encapsulated with graphene networks as a low-cost and large-scalable anode material for fast sodium storage with an ultralong cycle life, Inorg. Chem. Front. 7 (2020) 402–410.
[22] S. Ibraheem, X. Li, S.S.A. Shah, T. Najam, G. Yasin, R. Iqbal, S. Hussain, W. Ding, F. Shahzad, Tellurium triggered formation of Te/Fe-NiOOH nanocubes as an efficient bifunctional electrocatalyst for overall water splitting, ACS Appl. Mater. Interfaces 13 (2021) 10972–10978.
[23] Y. Li, J. Abbott, Y. Sun, J. Sun, Y. Du, X. Han, G. Wu, P. Xu, Ru nanoassembly catalysts for hydrogen evolution and oxidation reactions in electrolytes at various pH values, Appl. Catal. B: Environ. 258 (2019), 117952.
[24] L. Yao, N. Zhang, Y. Wang, Y. Ni, D. Yan, C. Hu, Facile formation of 2D Co2P@Co3O4 microsheets through in-situ toptactic conversion and surface corrosion: Bifunctional electrocatalysts towards overall water splitting, J. Power Sources 374 (2018) 142–148.
[25] W.-H. Lai, L.-F. Zhang, W.-B. Hua, S. Indris, Z.-C. Yan, Z. Hu, B. Zhang, Y. Liu, L. Wang, M. Liu, R. Liu, Y.-X. Wang, J.-Z. Wang, Z. Hu, H.-K. Liu, S.-L. Chou, S.-X. Dou, General π-electron-assisted strategy for Ir, Pt, Ru, Pd, Fe, Ni single-atom electrocatalysts with bifunctional active sites for highly efficient water splitting, Angew. Chem. Int. Ed. 58 (2019) 11868–11873.
[26] W. Luo, J. Gan, Z. Huang, W. Chen, G. Qian, X. Zhou, X. Duan, Boosting HER performance of Pt-Based catalysts immobilized on functionalized vulcan carbon by atomic layer deposition, Front. Mater. 6 (2019) 251.
[27] P. Guo, J. Wu, X.-B. Li, J. Luo, W.-M. Lau, H. Liu, X.-L. Sun, L.-M. Liu, A highly stable bifunctional catalyst based on 3D Co(OH)2@NCNTs@NF towards overall water-splitting, Nano Energy 47 (2018) 96–104.
[28] D. Kan, D. Wang, X. Zhang, R. Lian, J. Xu, G. Chen, Y. Wei, Rational design of bifunctional ORR/OER catalysts based on Pt/Pd-doped Nb2CT2 MXene by first-principles calculations, J. Mater. Chem. A 8 (2020) 3097–3108.
[29] J. Wang, Y. Fan, S. Qi, W. Li, M. Zhao, Bifunctional HER/OER or OER/ORR Catalytic Activity of Two-Dimensional TM3(HITP)2 with TM = Fe–Zn, J. Phys. Chem. C 124 (2020) 9350–9359.
[30] F. Song, L. Bai, A. Moysiadou, S. Lee, C. Hu, L. Liardet, X. Hu, Transition metal oxides as electrocatalysts for the oxygen evolution reaction in alkaline solutions: an application-inspired renaissance, J. Am. Chem. Soc. 140 (2018) 7748–7759.
[31] A. Loh, X. Li, O.O. Taiwo, F. Tariq, N.P. Brandon, P. Wang, K. Xu, B. Wang, Development of Ni–Fe based ternary metal hydroxides as highly efficient oxygen evolution catalysts in AEM water electrolysis for hydrogen production, Int. J. Hydrogen Energy 45 (2020) 24232–24247.
[32] L. Yu, S. Song, B. McElhenny, F. Ding, D. Luo, Y. Yu, S. Chen, Z. Ren, A universal synthesis strategy to make metal nitride electrocatalysts for hydrogen evolution reaction, J. Mater. Chem. A 7 (2019) 19728–19732.
[33] A. Dutta, N. Pradhan, Developments of metal phosphides as efficient OER precatalysts, J. Phys. Chem. Lett. 8 (2017) 144–152.
[34] R. Zahra, E. Pervaiz, M. Yang, O. Rabi, Z. Saleem, M. Ali, S. Farrukh, A review on nickel cobalt sulphide and their hybrids: earth abundant, pH stable electro-catalyst for hydrogen evolution reaction, Int. J. Hydrogen Energy 45 (2020) 24518–24543.
[35] X. Xia, L. Wang, N. Sui, V.L. Colvin, W.W. Yu, Recent progress in transition metal selenide electrocatalysts for water splitting, Nanoscale 12 (2020) 12249–12262.
[36] D. Siegmund, N. Blanc, M. Smialkowski, K. Tschulik, U.-P. Apfel, Metal-rich chalcogenides for electrocatalytic hydrogen evolution: activity of electrodes and bulk materials, ChemElectroChem 7 (2020) 1514–1527.
[37] S. Li, X. Hao, A. Abudula, G. Guan, Nanostructured Co-based bifunctional electrocatalysts for energy conversion and storage: current status and perspectives, J. Mater. Chem. A 7 (2019) 18674–18707.
[38] F. Yu, H. Zhou, Y. Huang, J. Sun, F. Qin, J. Bao, W.A. Goddard, S. Chen, Z. Ren, High-performance bifunctional porous non-noble metal phosphide catalyst for overall water splitting, Nat. Commun. 9 (2018) 2551.
[39] A. Kumar, S. Ibraheem, T. Anh Nguyen, R.K. Gupta, T. Maiyalagan, G. Yasin, Molecular-MN4 vs atomically dispersed M−N4−C electrocatalysts for oxygen reduction reaction, Coord. Chem. Rev. 446 (2021), 214122.
[40] S. Ibraheem, S. Chen, L. Peng, J. Li, L. Li, Q. Liao, M. Shao, Z. Wei, Strongly coupled iron selenides-nitrogen-bond as an electronic transport bridge for enhanced synergistic oxygen electrocatalysis in rechargeable zinc-O2 batteries, Appl. Catal. B: Environ. 265 (2020), 118569.
[41] Y. Sun, K. Xu, Z. Wei, H. Li, T. Zhang, X. Li, W. Cai, J. Ma, H.J. Fan, Y. Li, Strong electronic interaction in dual-cation-incorporated NiSe2 nanosheets with lattice distortion for highly efficient overall water splitting, Adv. Mater. 30 (2018), 1802121.
[42] M. Luo, H. Yu, F. Hu, T. Liu, X. Cheng, R. Zheng, Y. Bai, M. Shui, J. Shu, Metal selenides for high performance sodium ion batteries, Chem. Eng. J. 380 (2020), 122557.
[43] X. Peng, Y. Yan, X. Jin, C. Huang, W. Jin, B. Gao, P.K. Chu, Recent advance and prospectives of electrocatalysts based on transition metal selenides for efficient water splitting, Nano Energy 78 (2020), 105234.
[44] Y.-N. Zhou, Y.-R. Zhu, X.-Y. Chen, B. Dong, Q.-Z. Li, Y.-M. Chai, Carbon–based transition metal sulfides/selenides nanostructures for electrocatalytic water splitting, J. Alloy. Compd. 852 (2021), 156810.
[45] S. Ibraheem, S. Chen, J. Li, Q. Wang, Z. Wei, In situ growth of vertically aligned FeCoOOH-nanosheets/nanoflowers on Fe, N co-doped 3D-porous carbon as efficient bifunctional electrocatalysts for rechargeable zinc–O2 batteries, J. Mater. Chem. A 7 (2019) 9497–9502.
[46] A. Kumar, V.K. Vashistha, D.K. Das, S. Ibraheem, G. Yasin, R. Iqbal, T.A. Nguyen, R. K. Gupta, M. Rasidul Islam, M-N-C-based single-atom catalysts for H2, O2 & CO_2 electrocatalysis: activity descriptors, active sites identification, challenges and prospects, Fuel 304 (2021), 121420.
[47] L. Xia, H. Song, X. Li, X. Zhang, B. Gao, Y. Zheng, K. Huo, P.K. Chu, Hierarchical 0D−2D Co/Mo selenides as superior bifunctional electrocatalysts for overall water splitting, Front. Chem. 8 (2020).
[48] Y. Dong, C.W. Oloman, E.L. Gyenge, J. Su, L. Chen, Transition metal based heterogeneous electrocatalysts for the oxygen evolution reaction at near-neutral pH, Nanoscale 12 (2020) 9924–9934.
[49] W.-J. Jiang, L. Gu, L. Li, Y. Zhang, X. Zhang, L.-J. Zhang, J.-Q. Wang, J.-S. Hu, Z. Wei, L.-J. Wan, Understanding the high activity of Fe–N–C electrocatalysts in oxygen reduction: Fe/Fe3C nanoparticles boost the activity of Fe–Nx, J. Am. Chem. Soc. 138 (2016) 3570–3578.
[50] J. Masa, P. Weide, D. Peeters, I. Sinev, W. Xia, Z. Sun, C. Somsen, M. Muhler, W. Schuhmann, Amorphous cobalt boride (Co2B) as a highly efficient nonprecious catalyst for electrochemical water splitting: oxygen and hydrogen evolution, Adv. Energy Mater. 6 (2016), 1502313.
[51] M. Arif, G. Yasin, M. Shakeel, M.A. Mushtaq, W. Ye, X. Fang, S. Ji, D. Yan, Highly active sites of NiVB nanoparticles dispersed onto graphene nanosheets towards

efficient and pH-universal overall water splitting, J. Energy Chem. 58 (2021) 237–246.
[52] W. Ye, Y. Yang, X. Fang, M. Arif, X. Chen, D. Yan, 2D cocrystallized metal–organic nanosheet array as an efficient and stable bifunctional electrocatalyst for overall water splitting, ACS Sustain. Chem. Eng. 7 (2019) 18085–18092.
[53] Q. Sun, Y. Tong, P. Chen, L. Chen, F. Xi, J. Liu, X. Dong, Dual anions engineering on nickel cobalt-based catalyst for optimal hydrogen evolution electrocatalysis, J. Colloid Interface Sci. 589 (2021) 127–134.
[54] X. Chang, T. Wang, P. Zhang, J. Zhang, A. Li, J. Gong, Enhanced surface reaction kinetics and charge separation of p–n heterojunction Co3O4/BiVO4 photoanodes, J. Am. Chem. Soc. 137 (2015) 8356–8359.
[55] R. Dholam, N. Patel, A. Santini, A. Miotello, Efficient indium tin oxide/Cr-doped-TiO2 multilayer thin films for H2 production by photocatalytic water-splitting, Int. J. Hydrogen Energy 35 (2010) 9581–9590.
[56] R. Jaiswal, J. Bharambe, N. Patel, A. Dashora, D.C. Kothari, A. Miotello, Copper and Nitrogen co-doped TiO2 photocatalyst with enhanced optical absorption and catalytic activity, Appl. Catal. B: Environ. 168 (2015) 333–341.
[57] Y. Jiang, P. Sun, L. Sharma, B. Mao, R. Kakkar, T. Meng, L. Zheng, M. Cao, Further insights into bifunctional mechanism in alkaline hydrogen evolution for hybridized nanocatalysts and general route toward mechanism-oriented synthesis, Nano Energy 81 (2021), 105645.
[58] Y. Wang, S. Tao, H. Lin, G. Wang, K. Zhao, R. Cai, K. Tao, C. Zhang, M. Sun, J. Hu, B. Huang, S. Yang, Atomically targeting NiFe LDH to create multivacancies for OER catalysis with a small organic anchor, Nano Energy 81 (2021), 105606.